VIBRATION MODES CHARACTERIZED BY RAYLEIGH WAVES PROPAGATING IN AN ELASTIC LAYER ON A RIGID BASE

By Shigeaki MORICHI*, Tatuso OHMACHI**, Takumi TOSHINAWA***
and Akiyo MIYAI****

Due to fact the that Rayleigh waves are attributed to a kind of natural vibration of a surface layer, their nature can be understood by vibration experiments using a shaking table or by vibration mode analysis of a layer of finite length. This has been confirmed experimentally, analytically and numerically. In the limiting case, where the wave length approaches infinity, the wave motion is found to be reduced to shear vibration and longitudinal vibration of the layer.

Keywords : Rayleigh wave, Model experiment, FEM, Quarter wave-length law

1. INTRODUCTION

Prediction of earthquake ground motions has been one of the major subjects in earthquake engineering. It is of special importance when civil structures or lifeline systems are to be built on a thick sedimentary layers, because surface waves of large amplitude and long duration are likely to develop in such layers. In this regard, earthquake records obtained by seismological array observations provide a valuable insight into the nature of such seismic ground motions[1]~[8].

In the meantime, it is also useful for us to understand the fundamental characteristics of surface motion by means of physical or numerical experiments in which we can easily control parameters associated with material properties and geometrical configrations. When we conduct physical experiments on transient wave propagation using a rather small-scale model, however, some difficulties arise in both detection of the surface motion and application of the desired force[9],[10]. This is also the case with a numerical analysis of a transient wave propagation in which special consideration should be paid to boundary conditions, and appropriate boundaries such as viscous boundaries[11] and transmitting boundaries[12] have been adopted. On the contrary, vibration experiments in which standing waveforms are observed can be more easily conducted, and resonant frequencies and vibration shapes resulting from the experiments can be directly compared with analytically obtained natural modes of vibration. Hence, we can say that the latter experiments have an advantage over the former if both experiments are equivalent. In this respect, we are encouraged to recall the similarity between waves and vibrations[14].

* Member of JSCE, Dr. Eng., Associate Professor, Science University of Tokyo (2641, Yamazaki, Higashi-kameyama, Noda-shi, Chiba).
** Member of JSCE, Dr. Eng., Associate Professor, Tokyo Institute of Technology (4259, Nagatsuta, Midori-ku, Yokohama).
*** Member of JSCE, M. Eng., Research Associate, Ditto.
**** M. Eng., NEC Software Hokuriku, Ltd. (1-6-3, Katamachi, Kanazawa)

From this point of view, the authors have demonstrated experimentally and analytically in their previous work that shear vibration modes of a surface layer are characterized by Love waves in the same layer[13),15)]. When one compares the formulation processes of the vibration modes and Love waves, they will readily become self-evident. On this basis, one can substitute steady-state shear vibration experiments for transient Love wave experiments. In this paper, a similar viewpoint is applied to characteristics of Rayleigh waves and the associated vibration modes.

2. EXPERIMENT

Every specimen used in this series of experiments is a model of an elastic layer on a rigid base. As model materials, acrylamide gel (Poisson's ratio is 0.5) and aluminium plate were used for the elastic layer and the base, respectively. For the sake of experimental convenience, both edges of each model were set to be either free or fixed. Dimensions, boundary conditions and shear wave velocities of models are shown in Table 1 and Fig. 1. Shear wave velocities were measured by subjecting specimens with the same mixture to resonant shear-vibration.

Each model was mounted on a shaking table and was excited horizontally by sinusoidal motion of the table. Various resonant responses produced in the vertical plane of the model were observed while the exciting frequency was gradually varied.

For models-A and -B, the predominanty induced components of displacement were horizontal in the lower frequency range and vertical in the higher frequency range. From the stationary waveforms observed in the vertical plane, nodal planes of horizontal motion were clearly distinguished, increasing in number with an increases in frequency. The same could be said regarding nodal planes of vertical motion. In the case of model-C, only vertical components of resonant responses along the central line in an exciting direction were observed for the sake of experimental convenience.

Photo 1 shows some examples of experimental results on model-A. Resonant responses shown in Photo 1-(1), -(4) and -(5) are quite similar to the

Table 1   Dimensions and boundary conditions of models.

Model	Height (mm)	Length (mm) (B.C.)	Width (mm) (B.C.)	Shear wave velocity (cm/s)
A	80	600 (Fixed)	80 (Free)	2.1×10^2
B	100	600 (Fixed)	100 (Free)	2.1×10^2
C	80	600 (Fixed)	600 (Fixed)	2.2×10^2

Fig. 1   Dimensions of model-C.

(1) $f=7.39$ Hz, $k=0.5$ ($\times 2\pi/60$ cm)

(2) $f=10.4$ Hz, $k=1.5$ ($\times 2\pi/60$ cm)

(3) $f=16.2$ Hz, $k=5.0$ ($\times 2\pi/60$ cm)

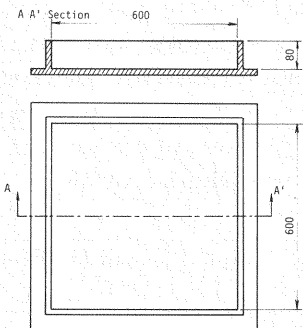(4) $f=17.9$ Hz, $k=0.5$ ($\times 2\pi/60$ cm)
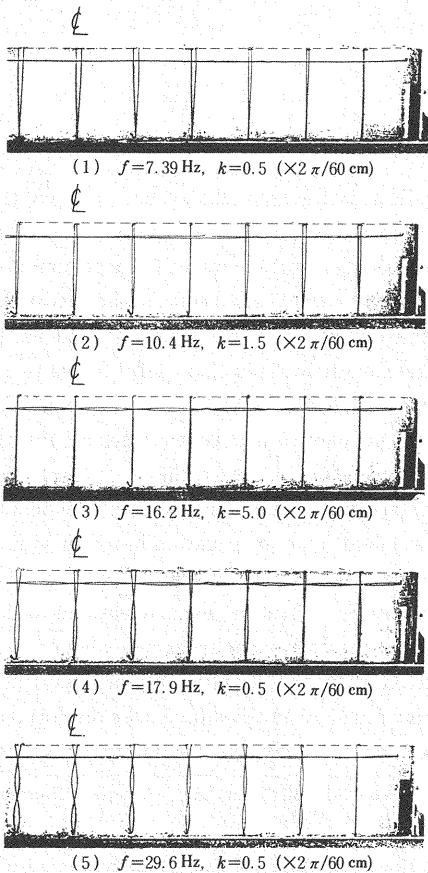
(5) $f=29.6$ Hz, $k=0.5$ ($\times 2\pi/60$ cm)

Photo 1   Experimental results.

responses caused by the shear vibration modes, and the vertical nodes of horizontal motion increase in number as the frequency increases. In addition, one antinodal plane of horizontal motion can be seen on the center line of **Photo 1-**(1), namely its wave number k is 0.5 ($\times 2\pi/60$ cm). According to **Photo 1-**(2), there are three antinodal planes of the horizontal component, and k becomes 1.5 ($\times 2\pi/60$ cm). **Photo 1-** (3) indicates that there are ten antinodes of the vertical component in the horizontal direction, that is, k $=5.0$ ($\times 2\pi/60$ cm).

For each observation, the phase velocity (C) of vertical or horizontal motion was calculated by multiplying frequency (f) and wave-length (λ) in the horizontal direction. Ratios of the phase velocity to the shear wave velocity (C/V_s) and the wave length to the model height (λ/H) are shown in **Table 2**. Relations between C/V_s and λ/H are plotted in **Fig. 2**, in which Rayleigh wave dispersion curves are also drawn. The reasonable accordance between experimental observation and theory shows that the observed resonant responses are characterized by Rayleigh waves.

Table 2 Experimental results.

Model	No.	Frequency f(Hz)	Wave number $k(\times 2\pi/60\text{cm})$	Wave length λ (cm)	Phase velocity $C = f \times \lambda$(cm/s)	Dimensionless Wave length λ/H	Dimensionless Phase velocity C/V_s
A	1	7.39	0.5(H)*	1.2×10^2	8.9×10^2	15	4.2
(H = 8.0cm)	2	10.4	1.5(H)	4.0×10	4.2×10^2	5.0	2.0
	3	11.8	3.0(V)**	2.0×10	2.4×10^2	2.5	1.1
	4	14.0	4.0(V)	1.5×10	2.1×10^2	1.9	1.0
	5	16.2	5.0(V)	1.2×10	1.9×10^2	1.5	0.90
	6	17.9	0.5(H)	1.2×10^2	2.1×10^3	15	10
	7	18.2	6.0(V)	1.0×10	1.8×10^2	1.3	0.86
	8	29.6	0.5(H)	1.2×10^2	3.6×10^3	15	17
B	1	6.85	0.5(H)	1.2×10^2	7.9×10^2	12	3.8
(H = 10.cm)	2	9.20	1.5(H)	4.0×10	3.7×10^2	4.0	1.8
	3	10.2	3.0(V)	2.0×10	2.0×10^2	2.0	0.95
	4	12.9	4.0(V)	1.5×10	1.9×10^2	1.5	0.90
	5	14.6	0.5(H)	1.2×10^2	1.8×10^3	12	8.6
	6	14.6	5.0(V)	1.2×10	1.8×10^2	1.2	0.86
	7	17.9	6.0(V)	1.0×10	1.8×10^2	1.0	0.86
	8	23.9	0.5(H)	1.2×10^2	2.9×10^3	12	14
	9	33.3	0.5(H)	1.2×10^2	4.0×10^3	12	19
C	1	13.3	2.0(V)	3.0×10^2	4.0×10^2	3.8	1.8
(H = 8.0cm)	2	15.4	3.0(V)	2.0×10^2	3.1×10^2	2.5	1.4
	3	17.2	4.0(V)	1.5×10^2	2.6×10^2	1.9	1.2
	4	19.5	5.0(V)	1.2×10^2	2.3×10^2	1.5	1.0
	5	22.7	6.0(V)	1.0×10^2	2.3×10^2	1.3	1.0
	6	30.5	5.0(V)	1.2×10^2	3.7×10^2	1.5	1.7

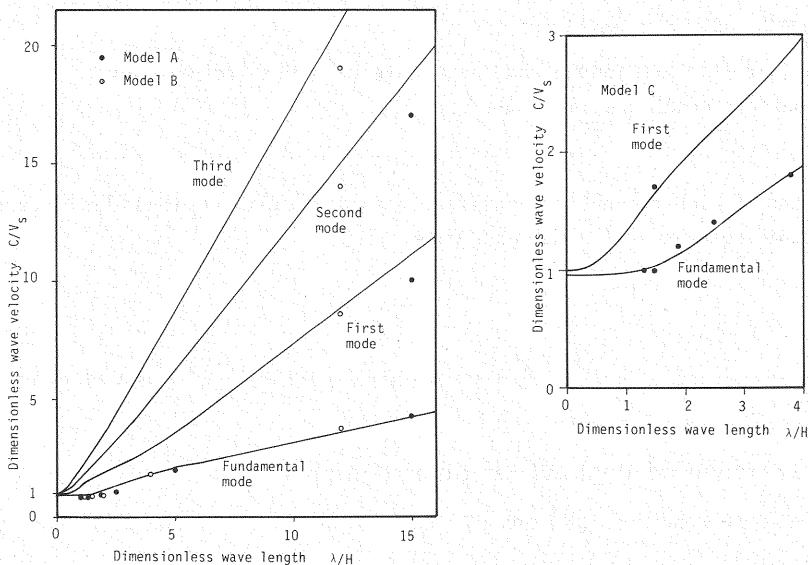*(H) Horizontal displacement,**(V) Vertical displacement

Fig. 2 Experimental results and Rayleigh wave dispersion curves.

3. DISCUSSIONS

(1) Theoretical approach

In order to examine the experimental results, discussion is made on eigenvalue solutions for an elastic layer lying on a rigid base with a horizontally infinite length. Let us assume that, on lines $00'$ and $11'$ shown in **Fig. 3**, only the vertical displacement is supressed.

Analytical model
F I G - 3
Fig. 3 Analytical model.

Boundary conditions are as follows;

$$w|_{x=0}=0, \quad w|_{x=L}=0, \quad u|_{z=0}=0, \quad w|_{z=0}=0, \quad \sigma_z|_{z=H}=0 \text{ and } \tau_{xz}|_{z=H}=0 \cdots\cdots\cdots\cdots\cdots (1)$$

where x and z are Cartesian coordinates, u and w are displacements in the x- and z-directions, σ_z denotes normal stress in the z-direction and τ_{xz} is the shearing stress.

From the eigenvalue analysis associated with the above boundary conditions[14], normal modes are given by the following expressions;

$$\left.\begin{array}{l} u=\left\{ C_1(\cosh rz-\cosh sz)+C_2\left(\sinh rz-\dfrac{sr}{k^2}\cdot\sinh sz\right)\right\}\cdot\cos kx\cdot\exp(i\omega t) \\[4mm] w=\dfrac{r}{k}\left\{ C_1\left(\sinh rz-\dfrac{k^2}{rs}\cdot\sinh sz\right)+C_2(\cosh rz-\cosh sz)\right\}\cdot\sin kx\cdot\exp(i\omega t) \end{array}\right\} \cdots\cdots (2)$$

where

$$C_2=-\frac{2\,rk\cdot\sinh rH-(k^2+s^2)\cdot\dfrac{k}{s}\cdot\sinh sH}{2\,rk\cdot\cosh rH-(k^2+s^2)\cdot\dfrac{r}{k}\cdot\cosh sH}\cdot C_1 \cdots\cdots\cdots\cdots\cdots\cdots\cdots (3)$$

alternatively

$$C_2=-\frac{\left[(r^2-k^2)+\dfrac{1-2\nu}{\nu}\cdot r^2\right]\cdot\cosh rH-\dfrac{1-2\nu}{\nu}\cdot k^2\cdot\cosh sH}{\left[(r^2-k^2)+\dfrac{1-2\nu}{\nu}\cdot r^2\right]\cdot\sinh rH-\dfrac{1-2\nu}{\nu}\cdot sr\cdot\sinh sH}\cdot C_1 \cdots\cdots\cdots\cdots (4)$$

In the above expressions, C_1, C_2, r, s and k are coefficients, ν means Poisson's ratio, ω denotes circular frequency, t is time and i is $\sqrt{-1}$. The relationships between r (or s) and k are;

$$r^2-k^2+\frac{\omega^2}{V_p^2}=0, \quad s^2-k^2+\frac{\omega^2}{V_s^2}=0 \cdots\cdots\cdots\cdots\cdots\cdots\cdots\cdots (5)$$

where V_p and V_s denote longitudinal and shear wave velocities, respectively.

From the boundary conditions, k should be;

$$k=\frac{n\pi}{L} \quad (n=1,2,\cdots)\cdots\cdots\cdots\cdots\cdots\cdots\cdots\cdots\cdots\cdots\cdots\cdots\cdots (6)$$

Taking (5) and (6) into account, circular frequency ω is calculated by the following expression, which is a characteristic equation of the Rayleigh wave.

$$2\,rk\cdot\left[(r^2-k^2)+\frac{1-2\nu}{\nu}\cdot r^2\right]$$

$$\times\left[1+\frac{\dfrac{1-2\nu}{\nu}}{(r^2-k^2)+\dfrac{1-2\nu}{\nu}\cdot r^2}\cdot\left(\frac{k^2+s^2}{2}+rs\cdot\sinh rH\cdot\sinh sH-k^2\cdot\cosh rH\cdot\cosh sH\right)\right.$$

$$\left.-\frac{k^2+s^2}{2\,rsk^2}\cdot(rs\cdot\cosh rH\cdot\cosh sH-k^2\cdot\sinh rH\cdot\sinh sH)\right]=0 \cdots\cdots\cdots\cdots\cdots (7)$$

For the plane stress condition, (4) and (7) could be obtained by replacing ν with $\dfrac{\nu}{1+\nu}$ and taking account of (5).

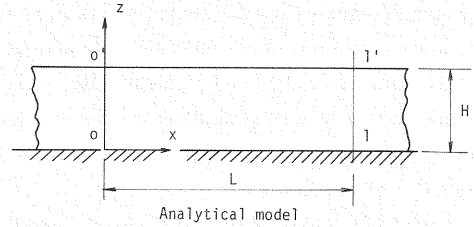Supposing that $2L/n$ and ω/k are the wave-length and phase velocity, respectively, of the stationary

wave, it becomes clear that the waves have the same dispersion characteristics as Rayleigh waves. The boundary conditions adopted in the experiments are slightly different from those in the theoretical approach. However, reasonable accordance between the experimental and theoretical results suggests that the difference in boundary conditions has less effect upon the wave characteristics.

Let us extend this discussion to an extreme condition. In the case of infinite wave-length, $k \rightarrow 0$, the expression in the second parenthesis of (7) becomes

$$\cosh rH \cdot \cosh sH = 0 \quad \cdots\cdots\cdots\cdots\cdots\cdots\cdots\cdots\cdots\cdots\cdots\cdots\cdots\cdots\cdots (8)$$

and the following are obtained by using (5),

$$r = i \cdot \frac{\omega}{V_p} \quad \cdots\cdots\cdots\cdots\cdots\cdots\cdots\cdots\cdots\cdots\cdots\cdots\cdots\cdots\cdots\cdots\cdots\cdots\cdots\cdots\cdots (9)$$

$$s = i \cdot \frac{\omega}{V_s} \quad \cdots\cdots\cdots\cdots\cdots\cdots\cdots\cdots\cdots\cdots\cdots\cdots\cdots\cdots\cdots\cdots\cdots\cdots\cdots\cdots (10)$$

Using (8) and (9), the frequency f or circular frequency ω is reduced to

$$f_n = \frac{\omega_n}{2\pi} = \frac{(2n+1)}{4H} \cdot V_p \quad (n = 0, 1, 2, \cdots) \cdots\cdots\cdots\cdots\cdots\cdots\cdots\cdots\cdots\cdots (11)$$

$$f_m = \frac{\omega_m}{2\pi} = \frac{(2m+1)}{4H} \cdot V_s \quad (m = 0, 1, 2, \cdots) \cdots\cdots\cdots\cdots\cdots\cdots\cdots\cdots\cdots\cdots (12)$$

According to (11) and (12), Rayleigh waves seem to have the same characteristics as longitudinal or shear vibrations of the layer, and are subject to the so-called quarter wave-length law at $k \rightarrow 0$. Evidently, the frequency f_m for $m=0$ always gives the fundamental frequency of a wave of infinite length. However, as for the higher order frequencies, we cannot tell which of $f_n (n \geqq 0)$ and $f_m (m \geqq 1)$ in (11) and (12) becomes smaller, because it depends on Poisson's ratio.

In the dispersion curve in **Fig. 2**, the gradient of a line linking the orgin and an arbitrary point on the curve is H/V_s times the frequency of the wave. Therefore, the lines with gradients H/V_s times f_n in (11) and f_m in (12) give asymptotes of the dispersion curve of each mode, respectively.

The phase velocity (C_L) of a Love wave propagating in an elastic layer on a rigid base is

$$C_L = V_s \sqrt{1 + \left(\frac{2m+1}{4} \cdot \frac{\lambda}{H}\right)^2} \quad (m = 0, 1, 2, \cdots) \cdots\cdots\cdots\cdots\cdots\cdots\cdots\cdots (13)$$

As $\lambda/H \rightarrow \infty$,

$$f_m = \frac{C_L}{\lambda} = \frac{2m+1}{4H} \cdot V_s \cdots\cdots\cdots\cdots\cdots\cdots\cdots\cdots\cdots\cdots\cdots\cdots\cdots\cdots\cdots\cdots\cdots (14)$$

According to the above, asymptotes of Rayleigh wave dispersion curves concerning f_m in (12) are found to give ones of Love wave dispersion curves.

In addition to the frequency characteristics of the Rayleigh waves at $k \rightarrow 0$, it is also interesting to examine the natural mode shape in (2). The first examination is for the case where the frequency is determined by (12). Using (2) and (3), and neglecting higher orders of k in comparison with k itself lead to the following amplitude ratio between $|u|$ and $|w|$.

$$\frac{|u|}{|w|} = \frac{\left| \cosh rz - \cosh sz + \tanh sH \cdot \left(1 - \frac{2r}{s} \cdot \frac{\sinh rH}{\sinh sH}\right) \cdot \sinh sz \right|}{\left| \frac{r}{k} \cdot \sinh rz \right|} \cdots\cdots\cdots\cdots\cdots (15)$$

Taking into account (10) and (12), at $k \rightarrow 0$, $\sinh sz$ and $\tanh sH$ approach $i \cdot \sin \{(2m+1)z/2H\}$ and $i \cdot \tan \{(2m+1)\pi/2\}$, respectively. Although the denominator also approaches infinity at $k \rightarrow 0$, the munerator approaches it more rapidly than the denominator, giving $|u| \gg |w|$. Thus, the mode shape in this case is found to approach that of shear vibration of the layer. The second examination is in the case where the frequency is determined by (11). Similarly to the above, from (2) and (4), an amplitude ratio between $|w|$ and $|u|$ results in;

$$\frac{|w|}{|u|}=\frac{\left|\cosh sz-\cosh rz+\tanh rH\cdot\left(1-\frac{1-2\nu}{1-\nu}\cdot\frac{s}{r}\cdot\frac{\sinh sH}{\sinh rH}\right)\cdot\sinh rz\right|}{\left|\frac{s}{k}\cdot\sinh sz\right|} \quad\cdots\cdots\cdots\cdots\cdots (16)$$

Using (9) and (11) and considering rapidity of convergence lead to $|w|\gg|u|$ and a harmonic variation of w in the vertical direction, which indicates that the mode shape in this case approaches that of longitudinal vibration of the layer.

Table 3 shows the lowest three mode shapes calculated in the vertical direction for $\nu=0.5$, and $\lambda/H=15$ and infinity. It can be seen that the horizontal component for λ/H $=15$ resembles the shear vibration mode shape represented by that for $\lambda/H=\infty$, and that the nodes in the vertical direction increase in number for higher modes. These can be confirmed in Photo 1-(1), -(4) and -(5) of the experiments in which Poisson's ratio ν was 0.5. When it comes to the experimental results shown in Table 2 or Fig. 2, it should be noticed that mode shapes of shorter wave lengths could be visually observed only in the fundamental mode. In other words, mode shapes of longer wave lengths only are visually observable in the expeiments. This would indicate that the response of the elastic layer to the basement motion decreases in amplitude with an in-crease in the mode number, as was demonstrated for vibration modes previously characterized by Love waves[15].

Table 3   Mode shape in a vertical direction ($\lambda/H=15$).

		Fundamental mode		First mode		Second mode	
		Horizontal	Vertical	Horizontal	Vertical	Horizontal	Vertical
Surface	0	1.000 (1.000)	0.274 (0.000)	−1.000 (−1.000)	0.076 (0.000)	1.000 (1.000)	0.051 (0.000)
	1	0.994 (0.981)	0.222 (0.000)	−0.835 (−0.832)	0.126 (0.000)	0.561 (0.556)	0.007 (0.000)
	2	0.946 (0.924)	0.171 (0.000)	−0.403 (−0.383)	0.159 (0.000)	−0.373 (−0.383)	0.001 (0.000)
	3	0.858 (0.832)	0.123 (0.000)	0.154 (0.195)	0.166 (0.000)	−0.976 (−0.981)	0.040 (0.000)
	4	0.735 (0.707)	0.082 (0.000)	0.651 (0.707)	0.144 (0.000)	−0.716 (−0.707)	0.088 (0.000)
	5	0.580 (0.556)	0.047 (0.000)	0.923 (0.981)	0.101 (0.000)	0.175 (0.195)	0.104 (0.000)
	6	0.400 (0.383)	0.021 (0.000)	0.881 (0.924)	0.053 (0.000)	0.903 (0.924)	0.073 (0.000)
	7	0.204 (0.195)	0.005 (0.000)	0.536 (0.556)	0.015 (0.000)	0.882 (0.832)	−0.023 (0.000)
Bottom	8	0.000 (0.000)	0.000 (0.000)	0.000 (0.000)	0.000 (0.000)	0.000 (0.000)	0.000 (0.000)

Note(1): * U(z):Horizontal component in a vertical direction
{u}=U(z)·cos kx
** W(z):Vertical component in a vertical direction
{w}=W(z)·sin kx
{ }:amplitude, x,z:Cartecian coordinate,k:wave number
Note(2): (   ):λ/H= ∞

Table 4   Boundary conditions on model egdes.

Model	Displacements on AA' and BB'		Note
	Vertical	Horizontal	
a	Fixed	Free	A' ─────────── B' ↓ 80 mm
b	Free	Fixed	
c	Fixed	Fixed	A ── 600 mm ── B

(2)   Numerical approach

In the experiments both side edges of the models were fixed, while in the theoretical approach they were vertically fixed and horizontally free. These boundary conditions were selected for the sake of experimental and theoretical convenience. Therefore, the above comparison is slightly incorrect, strictly speaking. In order to examine the influence of the difference in boundary conditions, eigenvalue analyses were conducted by the finite element method. Models and boundary conditions used in the analyses are shown in Table 4. The height and width of each model are 8 cm and 60 cm, respectively. Model-a in Table 4 has the same boundary conditions as that for the theoretical approach. As shown in (2), u lags w by a phase difference of $90°$ with respect to kx, then model-b was used as the complement of model-a. Model-c has same boundary conditions as those of the experimental models (models-A and -B). Using the finite element program Isas-II (Integrated Structural Analysis System II)[16] natural modes of vibration of these models were calculated for Poisson's ratio 0.25 and shear wave velocity of 280 cm/s, as an example.

Fig. 4 shows the numerically obtained mode shape of model-a. The vertical component of the vibration mode shape is seen to have six nodes in a horizontal direction, and two nodes in a vertical direction. As for the horizontal component, it has three nodes in a vertical direction. These vibration mode shapes coincide very well with the theoretical mode shapes of the Rayleigh wayes shown in the upper part of Fig. 4. Such good accordance could also be seen in most other modes, especially in the lower modes, calculated for models-a, -b and -c.
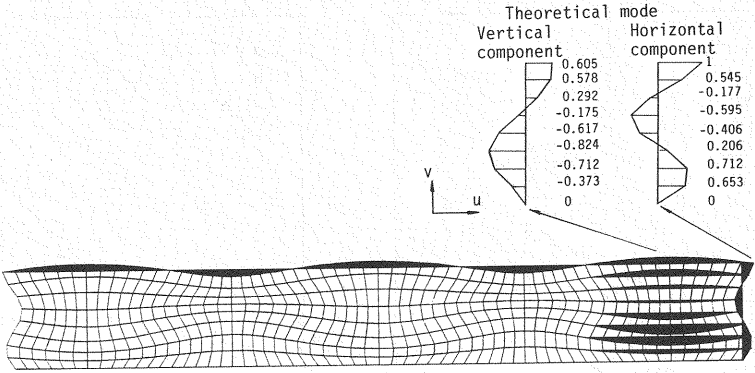
Fig. 4 A numerically obtained mode shape and theoretical mode shape.

Table 5 Numerical results.

No.	Mode number			Natural frequency f (Hz)			Number of nodes		Wave number k (×2π/60cm)	Wave length λ (cm)	Phase velocity C=f(a or b)×λ (cm/s)	Dimensionless wave length λ/H	Dimensionless phase velocity C/Vs
	a	b	c	a	b	c	A	B					
1	1	–	–	8.736	–	–	1	0	0 (H)**	∞	∞	∞	∞
2	2	1	1	9.538	9.538	9.544	1	*	0.5(H)	120.0	1145	15.00	4.089
3	3	2	2	11.61	11.61	11.63	1	*	1.0(H)	60.00	696.6	7.500	2.488
4	4	3	3	14.40	14.40	14.43	1	2	1.5(H)	40.00	576.0	5.000	2.057
5	11	11	10	17.54	17.54	17.59	1	2	2.0(H)	30.00	526.2	3.750	1.879
6	14	14	13	20.84	20.84	20.92	1	2	2.5	24.00	500.2	3.000	1.786
7	17	17	16	24.20	24.20	24.29	1	2	3.0	20.00	484.0	2.500	1.729
8	23	22	21	27.52	27.52	27.65	1	2	3.5	17.14	471.7	2.143	1.685
9	26	25	24	30.74	30.74	30.91	1	2	4.0	15.00	461.1	1.875	1.647
10	31	30	29	33.77	33.77	33.98	1	2	4.5	13.33	450.2	1.667	1.608
11	34	33	32	36.54	36.54	36.79	1	2	5.0	12.00	438.5	1.500	1.566
12	37	36	35	38.99	38.99	39.23	2	2	5.5	10.91	425.4	1.364	1.519
13	43	42	40	41.17	41.17	41.27	2	2	6.0	10.00	411.7	1.250	1.470
14	--	49	--	--	43.14	--	2	2	6.5	9.231	398.2	1.154	1.422
15	--	7	--	--	15.13	--	0	1	0 (V)***	∞	∞	∞	∞
16	6	5	4	15.09	15.09	15.09	2	1	0.5	120.0	1811	15.00	6.468
17	5	4	5	15.04	15.04	15.11	2	1	1.0	60.00	902.4	7.500	3.223
18	7	6	6	15.12	15.12	15.31	2	1	1.5	40.00	604.8	5.000	2.160
19	8	8	7	15.47	15.47	15.75	2	1	2.0	30.00	464.1	3.750	1.658
20	9	9	8	16.14	16.14	16.47	2	1	2.5	24.00	387.4	3.000	1.384
21	10	10	9	17.11	17.11	17.47	2	1	3.0	20.00	342.2	2.500	1.222
22	12	12	11	18.37	18.37	18.71	2	1	3.5	17.14	314.9	2.143	1.125
23	13	13	12	19.85	19.85	20.15	2	1	4.0	15.00	297.8	1.875	1.064
24	15	15	14	21.50	21.50	21.76	2	1	4.5	13.33	286.6	1.667	1.024
25	16	16	15	23.30	23.30	23.50	2	1	5.0	12.00	279.6	1.500	0.9986
26	18	18	17	25.19	25.19	25.32	2	1	5.5	10.91	274.8	1.364	0.9814
27	21	20	19	27.15	27.15	27.24	2	1	6.0	10.00	271.5	1.250	0.9696
28	25	24	23	29.16	29.16	29.22	2	1	6.5	9.231	269.2	1.154	0.9614
29	28	27	26	31.21	31.21	31.27	2	1	7.0	8.571	267.5	1.071	0.9554
30	30	29	28	33.29	33.29	33.36	2	1	7.5	8.000	266.3	1.000	0.9511
31	32	31	30	35.37	35.37	35.46	2	1	8.0	7.500	265.3	0.9375	0.9475
32	35	34	33	37.47	37.47	37.57	2	1	8.5	7.058	264.5	0.8823	0.9446
33	38	37	36	39.55	39.55	39.69	2	1	9.0	6.667	263.7	0.8334	0.9418
34	46	45	43	41.64	41.64	41.82	2	1	9.5	6.316	263.0	0.7895	0.9393
35	--	--	50	--	--	44.00	2	1	10	--	--	--	--
36	19	--	--	25.87	--	--	2	0	0 (H)	∞	∞	∞	∞
37	20	19	18	26.25	26.25	26.24	2	1	0.5(H)	120.0	3150	15.00	11.25
38	22	21	20	27.32	27.32	27.32	2	1	1.0(H)	60.00	1639	7.500	5.854
39	24	23	22	28.92	28.92	28.96	2	1	1.5(H)	40.00	1157	5.000	4.132
40	27	26	25	30.90	30.90	30.95	2	1	2.0(H)	30.00	927.0	3.750	3.311
41	29	28	27	33.14	33.14	33.19	2	1	2.5	24.00	795.4	3.000	2.841
42	33	32	31	35.56	35.56	35.60	2	1	3.0	20.00	711.2	2.500	2.540
43	36	35	34	38.12	38.12	38.13	2	1	3.5	17.14	653.4	2.143	2.334
44	39	38	37	40.75	40.75	40.71	2	1	4.0	15.00	611.3	1.875	2.183
45	--	50	47	--	43.46	43.27	2	1	4.5	13.33	579.3	1.667	2.069
46	48	--	--	42.02	--	--	3	0	0 (H)	∞	∞	∞	∞
47	47	46	44	41.79	41.79	41.83	3	2	0.5(H)	120.0	5015	15.00	17.91
48	44	43	41	41.38	41.38	41.39	3	2	1.0(H)	60.00	2483	7.500	8.868
49	42	41	39	41.06	41.06	41.05	3	2	1.5(H)	40.00	1642	5.000	5.864
50	40	39	38	40.93	40.93	41.00	3	2	2.0	30.00	1228	3.750	4.386
51	41	40	--	41.04	41.04	--	3	2	2.5	24.00	985.0	3.000	3.518
52	45	44	--	41.41	41.41	--	3	2	3.0	20.00	828.2	2.500	2.958
53	49	47	--	42.07	42.07	--	3	2	3.5	17.14	721.1	2.143	2.575
54	50	48	--	43.06	43.06	--	3	2	4.0	15.00	645.9	1.875	2.307

* uncertain,**(H) Horizontal component is predominant,***(V) Vertical component is predominant

In Table 5, the results of the numerical analysis are summarized to compare the modal characteristics of each model. Numbers in the second through fourth columns of the table indicate the order of each mode from the lowest one. A and B in the eighth and ninth columns indicate the number of nodes of horizontal and
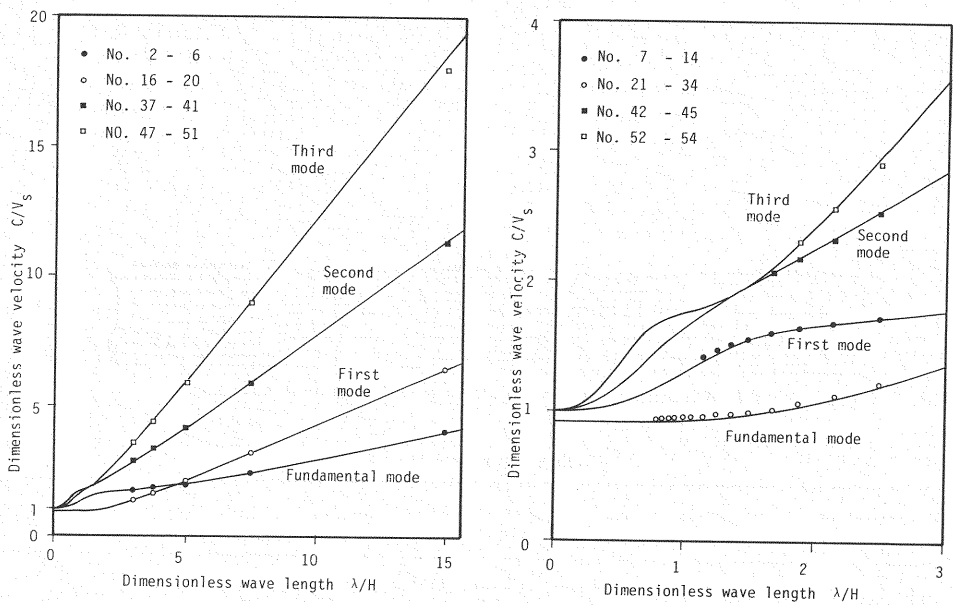
Fig. 5 Relation between phase velocity and wavelength of the numerically obtained vibration modes.

vertical components, respectively, counted in the vertical direction. Notation k in the tenth column means wave number of horizontal or vertical components measured in the horizontal direction. In the table, it seems natural that almost all the modal frequencies of model-c should be slightly higher than those of models-a and -b because of its displacement restraint at both side edges.

Table 6 Natural frequency of the modes with infinite wave-length.

No.	Numerical analysis	Quarter wave-length law
1	8.736 (Hz)	8.750 (Hz)
36	25.87	26.25
46	42.02	43.75
15	15.13	15.16

Dimensionless quantities in the two far right columns of Table 5 are plotted in Fig. 5 together with dispersion curves of Rayleigh waves. It is evident in Fig. 5 that every plotted point falls on the dispersion curves, which shows that the vibration modes are practically characterized by the Rayleigh waves.

The modes described in rows No. 1, 36 and 46 of Table 5 have only a horizontal component of displacement without a vertical component, and the number of nodes in the vertical direction increases with an increase in the frequency.

Meanwhile, the mode in row No. 15 has only a vertical component of displacement. Using $V_s=280$ cm/s and $V_p=485$ cm/s of the model material, frequencies of shear and longitudinal vibration were calculated by the quarter wave-length law expressed in (11) and (12), with results shown in Table 6, in which frequencies from the numerical analyses are also shown.

The fairly good agreement between each pair of frequencies is a statement of the fact that the numerically obtained modes of vibration are those of the shear and longitudinal vibration, and that they are characterized by Rayleigh waves even in the limiting case of $k=0$.

4. CONCLUSIONS

The natural modes of vibration of a surface layer lying on a rigid base were evaluated by laboratory experiments followed by theoretical and numerical analyses. Comparison of the mode shapes and frequencies were made between them, giving the following conclusions ;

(1) Natural modes of vibration of the surface layer of finite length evaluated under the plane strain conditions are characterized by Rayleigh waves in the layer. The only difference between the modes of vibration and those of Rayleigh waves is that the former is discrete while the latter is continuous regarding

their frequency, wave number, wave-length and so forth.

（2） In the limiting case where the wave-length of the Rayleigh wave is infinite, the Rayleigh wave is reduced to shear or longitudinal vibration of the layer, and its natural frequencies are subjected to the quarter wave-length law.

（3） For these reasons, vibration experiments on the surface layer can serve as useful means of deepening our understanding of Rayleigh wave characteristics, because they are adapted to our visual observation.

（4） Restraint of displacement at side edges has little effect on the vibration modes, especially on the lower modes. This permits us to use simple models whose side edges are both fixed in the experiments, in stead of sophisticated models satisfying boundary conditions associated with the Rayleigh wave.

ACKNOWLEDGEMENT

REFERENCES

1) Tsuchida, H., Kurata, E. and Hayashi, S. : Observation of Earthquake Response of Ground with Horizontal and Vertical Seismometer Arrays, Proc. of the 6th World Conference of Earthquake Engineering (6th W. C. E. E.), Vol. 1, pp. 509~515, 1977.

2) Tsuchida et al. : Observation of Earthquake Response of Ground with Horizontal and Vertical Seismometer Arrays, Proc. of the 7th W. C. E. E. Vol. 2, pp. 475~482, 1980.

3) Muto, K. et al. : Analysis of Strong Motions Observed in Earthquake Instruments Arrays, Proc. of the 8th E. C. E. E., Vol. 2, pp. 159~166, 1984.

4) Nakamura, Y. and Saito, A. : Meandering Earthquake Motion of Soft Surface Ground, Proc. of the 8th W. C. E. E., Vol. 2, pp. 175~182, 1984.

5) Bolt, B. A., Abrahamson, N. and Yeh, Y. T. : The Variation of Strong Ground Motion over Short Distance, Proc. of the 8th W. C. E. E., Vol. 2, pp. 183~190, 1984.

6) Loh, C. H. and Penzien, J. : Identification of Wave Types, Directions and Velocities Using SMART-I Strong Motion Array Data, Proc. of the 8th W. C. E. E., Vol. 2, pp. 191~198, 1984.

7) Fukumori, Y. et al. : Detection of Dispersion Characteristics of Apparant Wave Velocity, Proc. of the 8th W. C. E. E., Vol. 2, pp. 223~230, 1984.

8) Narahashi, H. et al. : Spatial Correlations of the Ground Motion Recorded by the Strong Motion Earthquakes Instrument Arrays, Proc. of the 8th W. C. E. E., Vol. 2, pp. 239~246, 1984.

9) Graff, K. F. : Wave Motion in Elastic Solid., Ohio University Press, 1975.

10) The seismic Exploration Group of Japan : Experimental Studies in Generation and Propagation of Seismic Waves (in Japanese), 1976.

11) Lysmer, J. and Kuhlemeyer, R. L. : Finite Dynamic Model for Infinite Media, Proc. of A. S. C. E., Vol. 95, EM4, pp. 859~877, 1969.

12) Kausel, E., Rosset, J. M. and Wass, G. : Dynamic Analysis of Footings on Layered Media, Jour. of Eng. Mech. Div. ASCE, Vol. 101, EM5, pp. 679~693, 1975.

13) Morichi, S., Ohmachi, T. and Tochinawa, T. : Vibration Modes Characterized by Love Waves in an Elastic Layer Overlying a Rigid Basement, Proc. of J. S. C. E. No. 356／I-3, pp. 203~211, Apr., 1985.

14) Sato, Y. : Elastic Wave Theory (in Japanese), Iwanami-shoten, 1978.

15) Ohmachi, T., Morichi, S. and Toshinawa, T. : Simplified Analysis procedure on Damped Vibration Equivalent to Love Waves in Double-layered Visco-elastic Media, Proc. of J. S. C. E., No. 374／I-6, pp. 239~247, Oct., 1986.

16) HITACHI : Manual 8080-7-142-10, 8080-7-112-20, 8080-7-135-10.